We are IntechOpen, the world's leading publisher of Open Access books Built by scientists, for scientists

4,800
Open access books available

122,000
International authors and editors

135M
Downloads

Our authors are among the

154
Countries delivered to

TOP 1%
most cited scientists

12.2%
Contributors from top 500 universities

CLARIVATE ANALYTICS BOOK CITATION INDEX INDEXED

WEB OF SCIENCE™

Selection of our books indexed in the Book Citation Index in Web of Science™ Core Collection (BKCI)

Interested in publishing with us?
Contact book.department@intechopen.com

Numbers displayed above are based on latest data collected.
For more information visit www.intechopen.com

Chapter 9

Time Dependent Behavior of Polymer Concrete Using Unsaturated Polyester Resin

Ghi Ho Tae and Eun Soo Choi

Additional information is available at the end of the chapter

http://dx.doi.org/10.5772/47181

1. Introduction

Time-dependent behavior of polyester-based materials such as polymer mortar or polymer concrete is recognized as an important aspect of mix design. Typically, creep and shrinkage of polyester-based materials exhibit complex time-dependent behavior. Thus, such time-dependent behavior is considered an essential design factor of the safety and serviceability of precast structures, especially during construction and at early age of curing. In the construction industry, the early age properties of polyester-based materials have become increasingly important because the use of rapidly cured materials can accelerate a construction process or shorten the production cycle of precast members [2,3]. The early age material properties of polyester-based materials, as influenced by setting shrinkage, have been investigated theoretically and experimentally. In some cases, the extent of setting shrinkage can significantly change the early age material properties and their development over time [4]. Recently, many polymer-based materials have been developed for potential civil engineering applications. Polymer concrete is one of the most promising materials. Polymer concrete has various advantages over conventional Portland cement concrete. They have higher compressive, tensile and flexural strengths. They also have fast curing time , an important advantage in many construction applications; polymer concrete materials cure in several hours or less, whereas Portland cement based materials take 2~4 weeks [5,8]. Also, they have excellent resistance to impact, abrasion, weathering, chemicals, water and salt sprays. However, the early age properties of these polymer concrete with unsaturated polyester resin have not been carefully investigated. Unsaturated polyester resins are used extensively as matrix materials in resin mortar systems. Conventional unsaturated polyester resins characteristically shrink about 5 to 10% by volume during curing process [1].

This shrinkage is unfavorable for molding properties despite the many excellent characteristics of the resins. Because the resin mortars have high elastic modulus and their

relatively low tensile strength owing to the high content of aggregates, the curing shrinkage is liable to induce cracks in molded parts [7,11]. It is well known that low shrinkage resin compounds consist of unsaturated polyester resins mixed with certain thermoplastics such as polystyrene, acrylic polymer, polyvinyl acetate, etc [13]. However, because low shrinkage behavior is complicated according to its dependent on many factors, such as components and curing conditions, several different hypotheses have been postulated [14].

In this study, shrinkage behaviors of recycled unsaturated polymer resin mortar were observed at the curing temperature, and creep tests on recycled unsaturated polymer resin concrete were carried out to achieve long term behaviors of creep. Results were extrapolated to develop a model that effectively creep characteristics from filler type, filler contents, and stress ratio and shrinkage mechanisms in recycled unsaturated polymer resin mortar were elucidate.

2. Experimental programs

2.1. Shrinkage experiment

2.1.1. Materials

The relevant details of the coarse and fine aggregates used are given in Table 1. The nature and properties of fillers are given in Table 2. The aggregate and fillers were dried in an oven at 110˚C(230F) for 24 hours prior to their use. The properties of montmorillonite are given in Table 3.

	Size(mm)	Ratio of Abrasion(%)	Specific gravity	Bulk specific gravity
Coarse	≤ 13	10.7	2.60	2.61
Fine	≤ 6	-	2.63	2.60
	S ize(mm)	Unit weight (N/mm^2)	Fineness modulus	Absorption (%)
Coarse	≤ 13	1,470,000	6.42	0.7
Fine	≤ 6	1,612,100	2.48	0.44

Table 1. Physical properties of aggregate

	Specific gravity	Fineness (cm^2/g)	Moisture (%)	PH	Absorption (%)
Flyash	2.2	3,765	0.2	-	-
$CaCO_3$	2.7	2,500~3,000	0.3	8.8	0.1

Table 2. Physical properties of fly ash and $CaCO_3$

	Specific gravity	L.B.D (kg/L)	Moisture (%)	pH	Sieve (%)
Spec.	-	0.75~0.85	0.2	10~11.5	Max.20
Result	1.22	0.8	0.3	10.4	18.9
Test Method	KS M 1104	KSM 0009		-	KS A 0507
Components	Recycled PET	Propylene glycol	Terephthalic acid	Styrene Monomer(SM)	OcCo
Percentage by whight	28.1	17.5	13.9	40	0.5

Table 3. Physical properties of Monmorillonite and polyester resin

2.1.2. Shrinkage measurement apparatus

A shrinkage measurement apparatus was specifically fabricated by modifying a commercially available length comparator (shrinkage measurement device conforming to BIS: 4031 – 1968), primarily used to measure the shrinkage of cement concrete and.. Shrinkage measurement devices were also devised earlier by Ohama, Stanley et al., and Dupont Company [9]. However, the modified length comparator was found to be more adaptable to the local laboratory conditions. A schematic diagram of the apparatus is shown in Fig. 1. It consists of two threaded circular rods, each of 25.4mm (1 in.) in diameter and 550mm (21.65 in.) in length. The threading was provided at both ends of each rod up to a length of 130mm (5.12in.). These rods were fixed to a channeled metallic frame (thickness 5.28mm [0.21 in.]) through bolts, and this frame was firmly fixed to a heavy table. Two cross plates, A and B, each of 0.002mm (78.7 micro in.) in sensitivity and 10mm (6.39 in.) in travel, were fixed at the middle of the two cross plates, A and B, respectively, such that the plungers of the dial gauges faced each other. A hole was provided at an appropriate place in the channeled frame so that the plunger of Dial Gauge B could protrude to come in contact with the test specimen. It was ensured that there was no hindrance of any kind to the movement of the plunger of Dial Gauge B when it passed through the hole in the frame. All the metallic parts of the device were made of mild steel. A preferred position could be to fix both cross plates on one side of the channeled frame, in which case no hole was needed in the frame. But the plates in this instance were placed on either side of the frame due to the limitations of rod lengths.

2.1.3. Shrinkage specimens

Polymer concrete specimens in this experiment were divided into three types. The first type consisted of 100mm square by 400mm bars for initial setting shrinkage, shown in Fig 2. The second type consisted of 25mm square by 285mm bars, whose mold is shown in Fig 3, tests setting shrinkage, coefficient of thermal expansion and strain by using the strain gauge inserted into above bars according to ASTM C531. And the last type is a φ75 ×

150mm cylinder, which was used to test the compressive strength of polymer concrete according to the content of montmorillonite. The proportions of binder and filler contents were varied, as shown in Table 4. The filler was mixed with the aggregate mixture and thoroughly dispersed. The binder, containing appropriate amounts of hardener and accelerator, was then added to the aggregate filler mixture, and a homogeneous polymer concrete mix was prepared. The dry coarse and fine aggregates were first added to the filler and montmorillonite in accordance with mix proportions and mixed for at least 2 minutes before adding unsaturated polyester resin. After mixing, Methy Ethyl Kepton Peroxide was slowly added in unsaturated polyester and was mixed for sufficiently long time. The mixture was poured slowly into the mixing equipment, which already contained the former mixture of aggregates, filler and montmorillonite. And final mixture was poured into respective appropriate molds to obtain a good mixture. The molds were then vibrated for 2 minutes to eliminate air voids in the mixture. The specimens were placed at room temperature for a day before demolding. The specimens demolded were placed at various temperatures and for various durations according to the experimental and material variables.

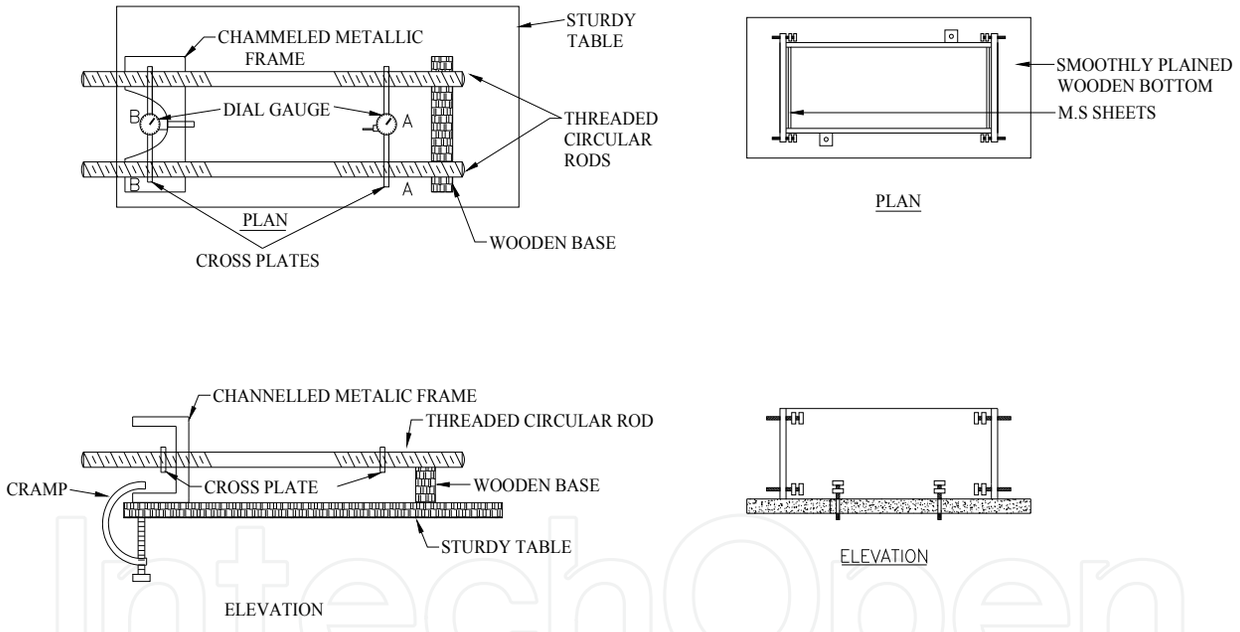

Figure 1. Shrinkage measuring device

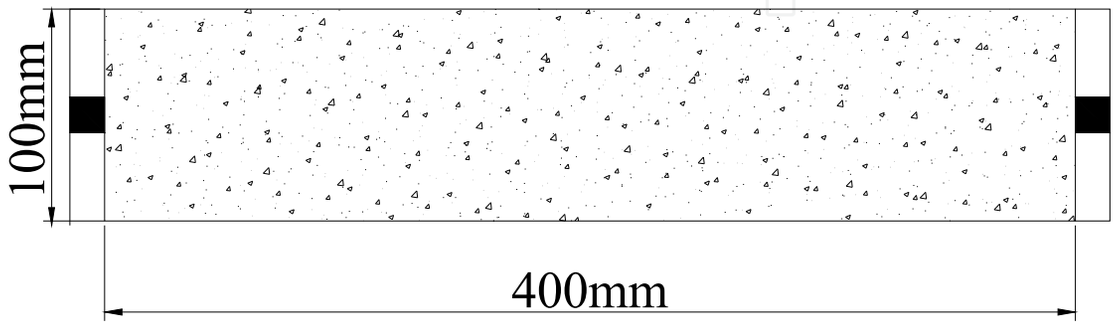

Figure 2. Sketch of mold of initial setting shrinkage

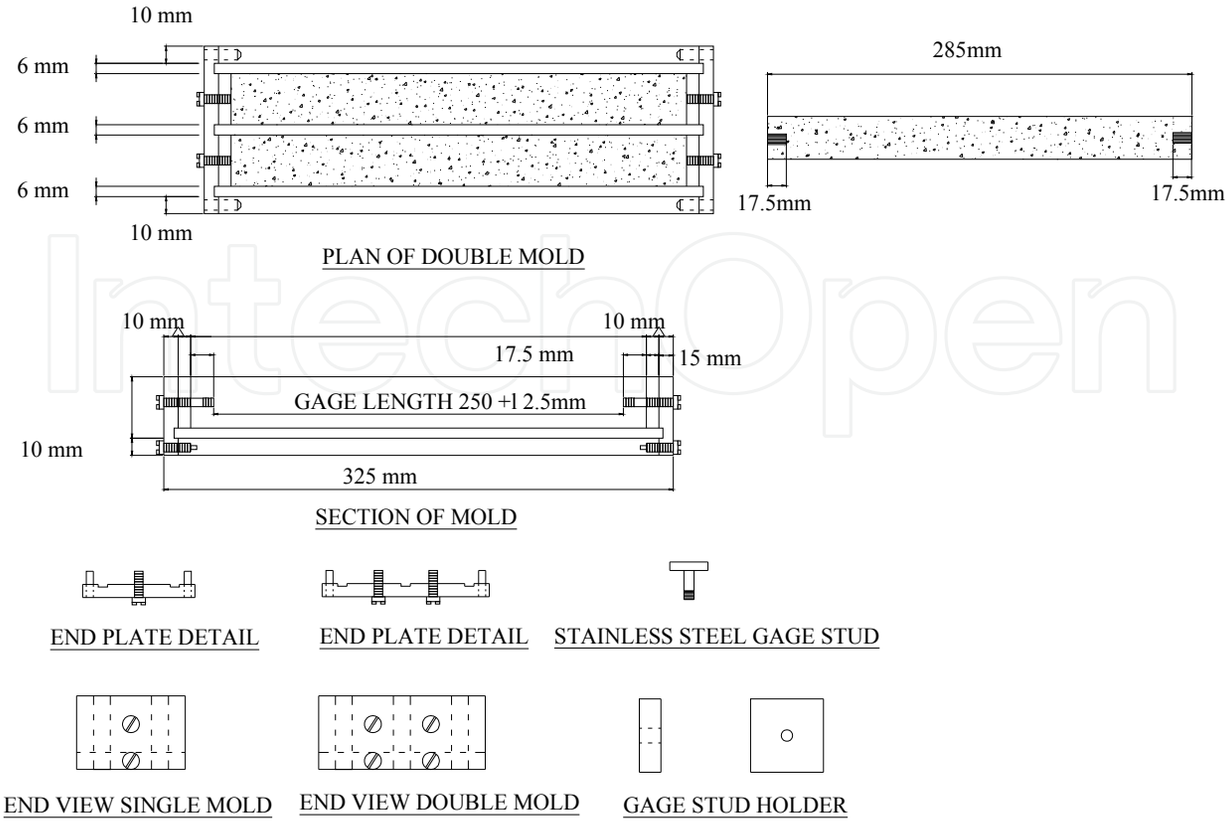

Figure 3. Sketch of mold of coefficient of thermal expansion

Specimens	Resin content (%)			Total Resin content(%)	Filler (%)	MMT (%)	Coarse Agg.	Fine Agg.
	UP	Mekpo	Total				<13mm	<6mm
PF	99	1	100	11	11	0	44	34
PFM2					10	2		
PFM4					8	4		
PFM6					6	6		
PFM8					4	8		
PFM10					2	10		
PFM12					0	12		
PC					11	0		
PCM5					6	5		

Table 4. Mix of Resin Paste

2.1.4. Curing method

30% methyl ethyl ketone peroxide (MEKPO) solution and 8% cobalt octoate (CoOc) solution were used as an initiator and an accelerator, respectively. The initiator and the accelerator were added in concentrations of 3.0 and 1.5 phr, respectively. N,N-dimethyl aniline (DMA) or acetyl acetone (AcAc) was employed to reduce curing time. These co-accelerator concentrations influenced the low shrinkage property of polyester resin. Furthermore, p-tertiary butyl catechol (PTBC) used as an inhibitor was kept at 20±1°C, the standard temperature before the addition of the initiator [6,10].

2.1.5. Measurements

The curing process of the resin mortar was continuously monitored by the strain gauge. The thermocouple embedded at the center of the test piece was removed so that the test piece could move freely. The curing process was monitored for over 24 hours. Measured values by the strain gauge were compared with the external dimension variations, as shown in Fig. 4. The exact relation between them was confirmed, though the measured values were 0.1% larger than the external dimension variations in either the expanded or shrunken state.

Figure 4. Strain gage setup for length change

The sides of the mold were opened immediately after the casing was completed. The specimen with the thin sheets at its ends was placed (along with wooden base) between the plungers of the dial gauges of the shrinkage- measurement device, and the initial readings were recorded. The entire casting operation took about 5 minutes.

The first readings in the dial gauges were treated as reference to calculate the shrinkage of polymer concrete. Subsequent readings on the dial gauges were taken after 20min, 30min, 1hr, 2hr, 3hr, 4hr, 5hr, 10hr, 15hr, 20hr, and 24hr of commencement of casting. During the period of the experiment, the laboratory temperature varied between 28 to 32C (82.4 to 89.6 F).

The change in length at one end of the specimen was calculated by multiplying the difference in dial gauge readings with the sensitivity of the dial gauge, i.e, 0.002mm. The total change in the length of the specimen would be the sum of the individual changes in length at both ends, calculated separately. The shrinkage of the specimen, in micro strains, was obtained by dividing the change in length of the specimen by its initial length [1,12].

2.2. Creep tests

The polymer concrete samples were mixed according to the polymer concrete test method 1.0 of the Society of Plastic Industry (referred to as SPI 1.0) [15]. The samples were mixed using a conventional concrete mixer for a period of about 3 min, poured into molds, vibrated, and cured at room temperature according to ASTM 1439 [16]. There are no standard tests that are directly applicable to polymer concrete specimens. Therefore, ASTM standards developed for cement were adopted as guidelines applicable. Polymer concrete cylinder specimens of 75mm diameter and 150mm height were tested in universal compression using hydraulic spring-loaded creep frames in the creep test room, which was equipped with temperature and humidity controls as shown in Fig.5. Electrical gages were bonded to the specimens at mid-height, and then connected to an automated data acquisition system. The short-term creep tests were carried out at 20°C, 30°C, and 40°C. Variables and specimen names are given in Table 5.

The temperature of the specimen was raised to the desired level and kept constant for 8h before the load was applied, in order to reach a stable temperature. The load was applied and kept constant for 24h. The strain was recorded before and after loading. At the end of the 24h the load was removed, the temperature was reduced to 20°C, and the specimens were allowed to recover for 16h from the creep strain before the temperature was raised to the next level (Fig. 6).

Fig.7 shows the stress level for the three short-term creep tests. Except for the stress ratio tests, the stress level f_0 was 20% of the ultimate compressive strength for short-term creep tests. The creep compliance curves of the 24h tests performed at elevated temperatures were used to predict the long-term creep compliance at 20°C. The creep strains were measured with concrete strain gages and recorded by an automated data acquisition system. The creep strains were recorded just after applied loading, every 10min for the first 1h, every 30min for the next 8h, and then every hour until the tests were finished.

Figure 5. Compressive creep test

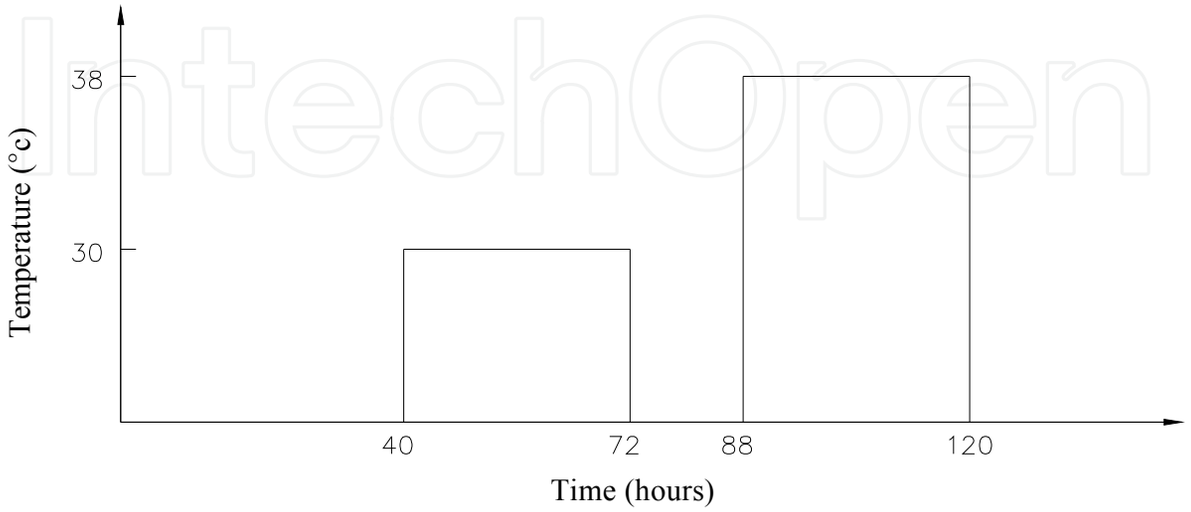

Figure 6. Temperature step for short-term creep test

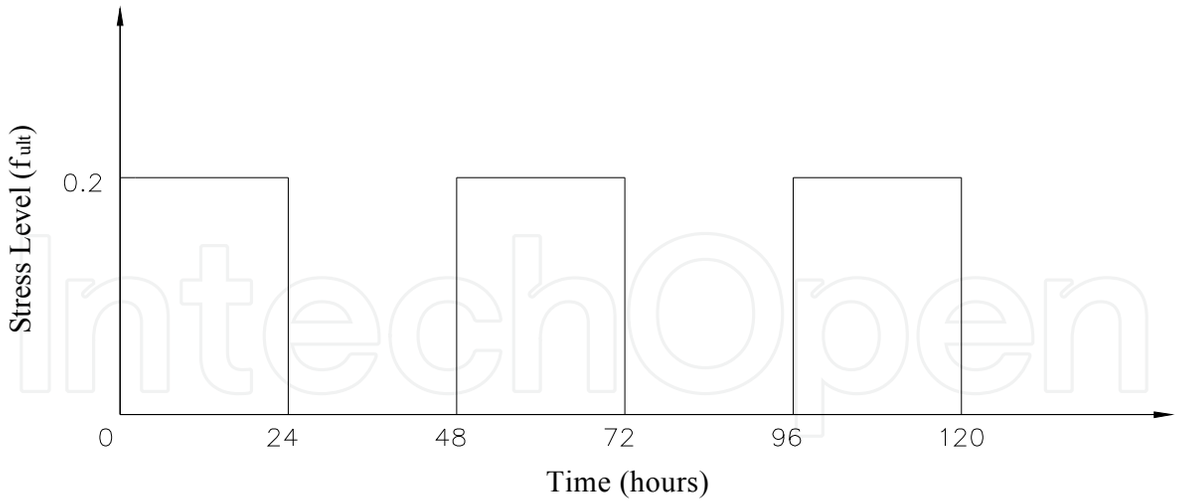

Figure 7. Stress level for short-term creep test

PC System	Classification	Change Factor
F-C-L20	Binder+ $CaCO_3$ 10%+Load 20%	Type of filler
F-Fa-L20	Binder+ Fly-ash 10%+Load 20%	
F-N-L20	Binder+ filler 0%+Load 20%	
F-C20-L20	Binder+ $CaCO_3$ 20%+Load 20%	Filler contents
F-C30-L30	Binder+ $CaCO_3$ 30%+Load 20%	
F-C-L30	Binder+ $CaCO_3$ 10%+Load 30%	Stress ratio
F-C-L40	Binder+ $CaCO_3$ 10%+Load 40%	

Table 5. Variables and names of specimens

2.3. Creep prediction method

A best way to achieve good long-term prediction is to conduct short-term creep tests on the given concrete and then extrapolate using Bayesian statistics [17]. A long-term creep compliance curve was constructed using the creep compliance curves of short-term creep tests performed at different temperatures. Based on the time-temperature analogy, a prediction was conducted using the results of short-term creep tests performed at 20°C, 30°C, and 40°C to predict the long-term creep compliance at 20°C [18,20].

This method takes the glassy creep compliance, measured at t=0 hours, and the 24-hour creep compliance values of each short-term creep test to develop a Prony series equation for the long-term creep compliance [22].

The creep compliance values at t=0 and t=24 are used to determine the coefficients of the following Prony series equation:

$$D(t) = D_g + D_1(1 - e^{-t/\tau_1}) \quad (1)$$

where D_g is the glassy creep compliance, which is measured at t=0. The retardation time τ_1 is set to the time coordinate t=24. The 24-hour creep compliance $D(t=24)$ is substituted in Eq. (1) and the coefficient D_1 is determined:

$$D_1 = 1.582\left[D(24) - D_g\right] \tag{2}$$

Eq. (2) is taken to determine the coefficient D_1 for each temperature. Coefficient D_1 is then substituted in Eq. (2) in order to develop a Prony series expression for each short-term creep compliance curve.

$$D^{20}(t) = D_g{}^{20} + D_1{}^{20}(1 - e^{-t/24}) \tag{3}$$

$$D^{30}(t) = D_g{}^{30} + D_1{}^{30}(1 - e^{-t/24}) \tag{4}$$

$$D^{40}(t) = D_g{}^{40} + D_1{}^{40}(1 - e^{-t/24}) \tag{5}$$

The superscripts 20, 30, and 40 indicate the temperature of the short-term creep compliance curve that each equation represents.

Eqs. (3), (4), and (5) are then used to develop the following expression for predicting the long-term creep compliance at 20°C:

$$D(t) = D^{20}(t) + D_{pred}(t) \tag{6}$$

where $D^{20}(t)$ is given by Eq. (3). The prediction term $D_{pred}(t)$ is given by two exponential terms:

$$D_{pred}(t) = D_2(1 - e^{-t/\tau_2}) + D_3(1 - e^{-t/\tau_3}) \tag{7}$$

where τ_2 and τ_3 are set at 1000 and 6000, respectively. The value of the exponential term $e^{-t/\tau}$ becomes zero when t increases above 4τ. The retardation constants τ_2 and τ_3 therefore have to be as large enough as that the exponential terms of Eq. (7) would have an effectively nonzero contribution to the long-term creep compliance predicted by Eq. (6).

It was observed that the coefficients of the exponential terms in Eqs. (3)–(5) increased with temperature. According to the time-temperature correspondence, increases in the value of the coefficients, i.e. an increase in the creep compliance, could have been caused either by a temperature or a time increase. The coefficients of the long-term 20°C curve, D_2 and D_3, are therefore expressed in terms of the coefficients of the 30°C curve and the 40°C curve, respectively, by the following expressions:

$$D_2 = rD_1{}^{30} \tag{8}$$

$$D_3 = rD_1^{40} \tag{9}$$

where r is the factor used to adjust the coefficients to minimize the error in the predicted creep compliance. The method of determining the parameter r is discussed below along with the presentation of the results [10].

Eqs. (3), (6), and (7) are substituted into Eq. (6) in order to develop the following equation that predicts the long-term creep compliance:

$$D(t) = D_g^{20} + D_1^{20}(1 - e^{-t/24}) + rD_1^{25}(1 - e^{-t/1000}) + rD_1^{30}(1 - e^{-t/6000}) \tag{10}$$

where the coefficients D_1^{20}, D_1^{30}, and D_1^{40} are determined by Eq. (4). Eq. (10) can predict the creep compliance values for times that do not exceed four times the larger retardation time, 6,000 hours. The predicted creep compliance value remains unchanged as time increases above 24,000 hours.

3. Results and discussion

To confirm the effectiveness of reinforcement, all results obtained from the specimens were compared with those from the control specimen. The following results are discussed: compressive and flexural strengths, thermal expansive coefficient, setting shrinkage for aging treatment, creep compliance, and predict model.

3.1. Compressive and flexural strengths

The effect of age on the compressive and flexural strength of recycled unsaturated polyester polymer concrete is shown in Fig. 8(a) and Fig. 8(b). Recycled unsaturated polyester resin-based polymer concrete achieves more than 80% of its 28-day strength in seven days. The high compressive strength of recycled unsaturated polyester resin-based polymer concrete allows the use of thinner sections in precast components, thus reducing dead loads in structures and minimizing transportation and erection costs. As a result, an increase in montmorillonite content from 1% to 5% increased the recycled unsaturated polyester polymer concrete compressive strength by about 12%. However, an increase in the montmorillonite content 8% decreased the strength of specimens.

The effect of temperature on the compressive and flexural strength of recycled unsaturated polyester polymer concrete is shown in Fig. 9. Fillers (fly ash, $CaCo_3$) were placed in an environmental chamber at the specified temperature 48 hr prior to mixing. After mixing, the specimens were again put in an environmental chamber at the designated temperature for a period of 28 days prior to testing. The selected temperatures were 20°C, 25°C, 30°C. Actual testing, performed at room temperature, was conducted immediately after removing the specimens from the environmental chamber. When the temperature increased, recycled unsaturated polyester polymer concrete lost strength because of the resulting loss in strength of the resin binder and the resulting decrease in bond strength between the inorganic aggregates and the resin binder. For example, Recycled unsaturated polyester

resin in temperature from 20°C to 30°C is more temperature sensitive than the inorganic cement binder used in producing normal Portland cement concrete. However, despite this loss in strength at high temperatures, Recycled unsaturated polyester polymer concrete remains at least twice as strong in compression as regular Portland cement concrete.

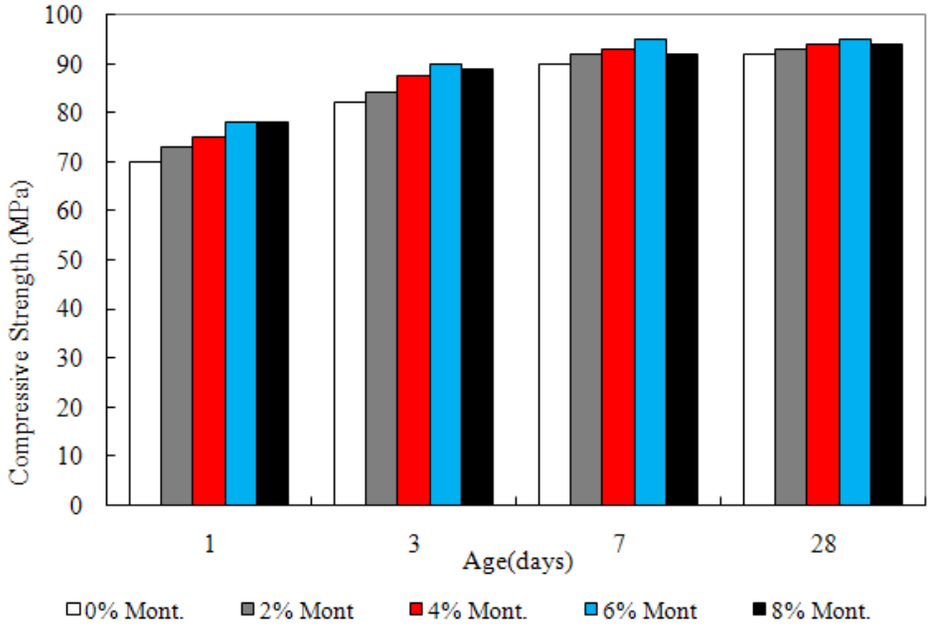

(a)

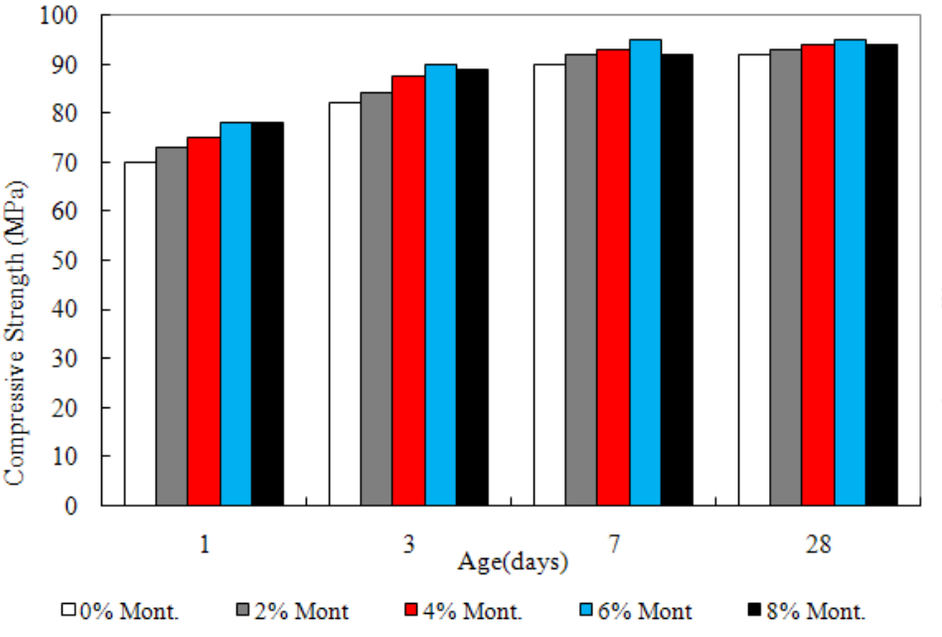

(b)

Figure 8. (a) Age effect on compressive strength, (b) Age effect on flexural strength

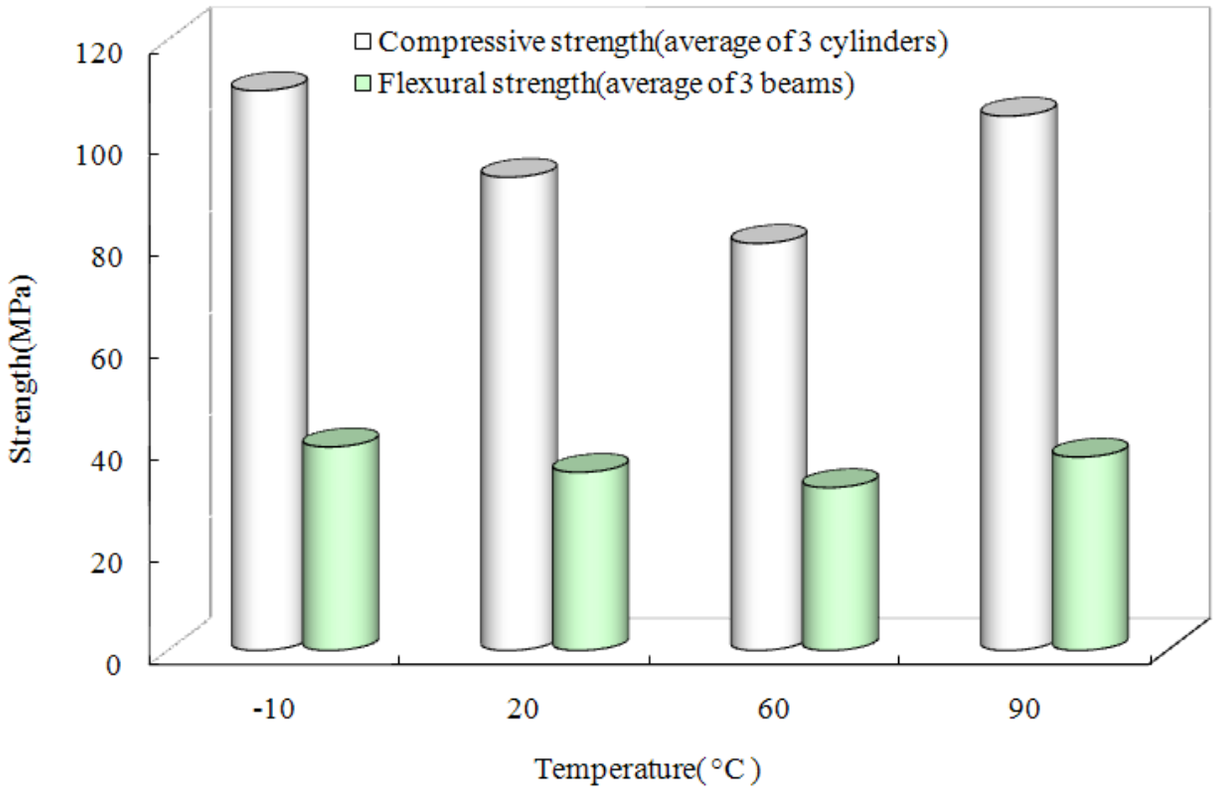

Figure 9. Temperature effect on compressive and flexural strength

3.2. Expansive coefficient

The thermal reaction of montmorillonite as the shrinkage reducing agent and fly ash and calcium carbonate as the filler is represented in Fig. 10.

The coefficient of thermal expansion decreases noticeably according to montmorillonite content. Moreover, specimens that used fly ash as the filler were less affected by temperature than those that used calcium carbonate among the specimens that contained 5% of montmorillonite evenly. The fact that fly ash is little sensitive to heat is useful when using polymer concrete made by recycled materials in construction materials. The coefficients of thermal expansion of polymer concrete produced by recycled PET maintained a good level than those of general polymer concrete ($2.5\sim3.5 \times 10^{-5}$) but showed a great difference from the coefficients of thermal expansion of general cement concrete ($0.7\sim1.2 \times 10^{-5}$).

The effect of curing temperature on specimens of montmorillonite 5% is shown in Fig. 11. The coefficient of thermal expansion decreased according to the increase of curing temperature because of the close up between polymer molecules and the complete hardening by high temperature during the initial curing process. Especially, the values from the specimens cured in water were relatively higher than those cured at high temperature.

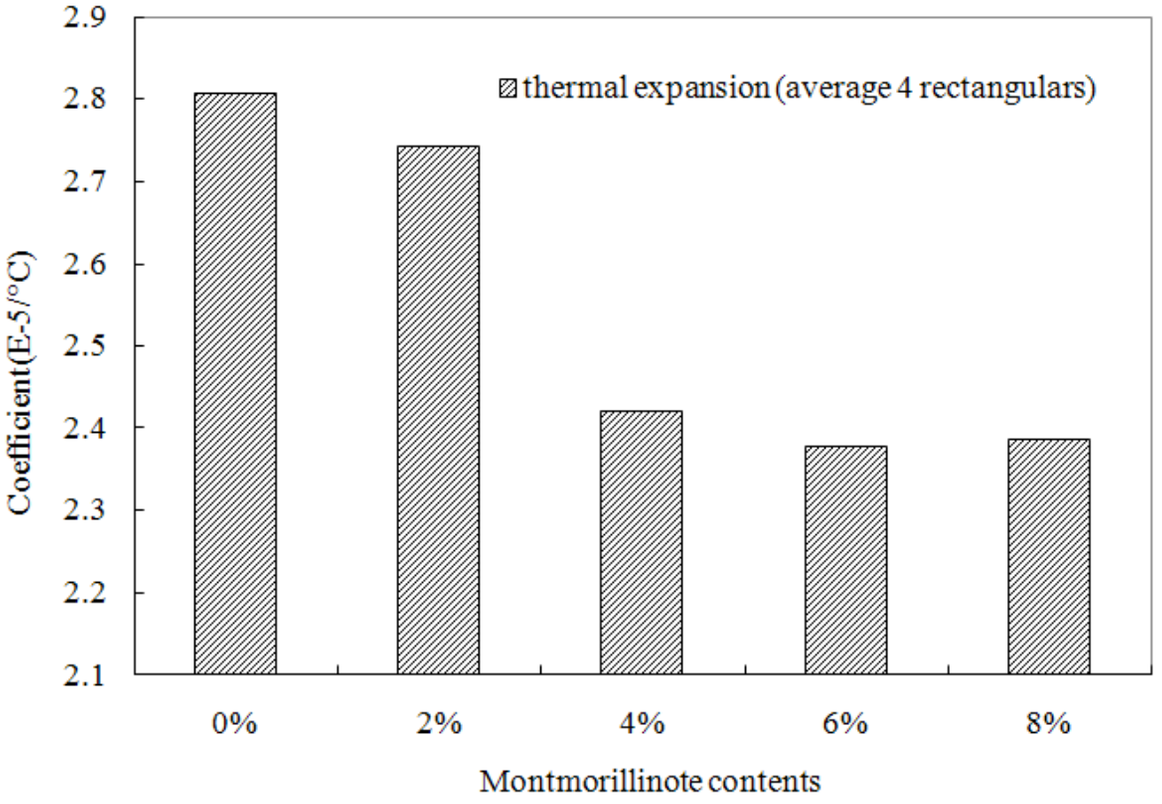

Figure 10. Coefficient of thermal expansion on montmorillonite contents

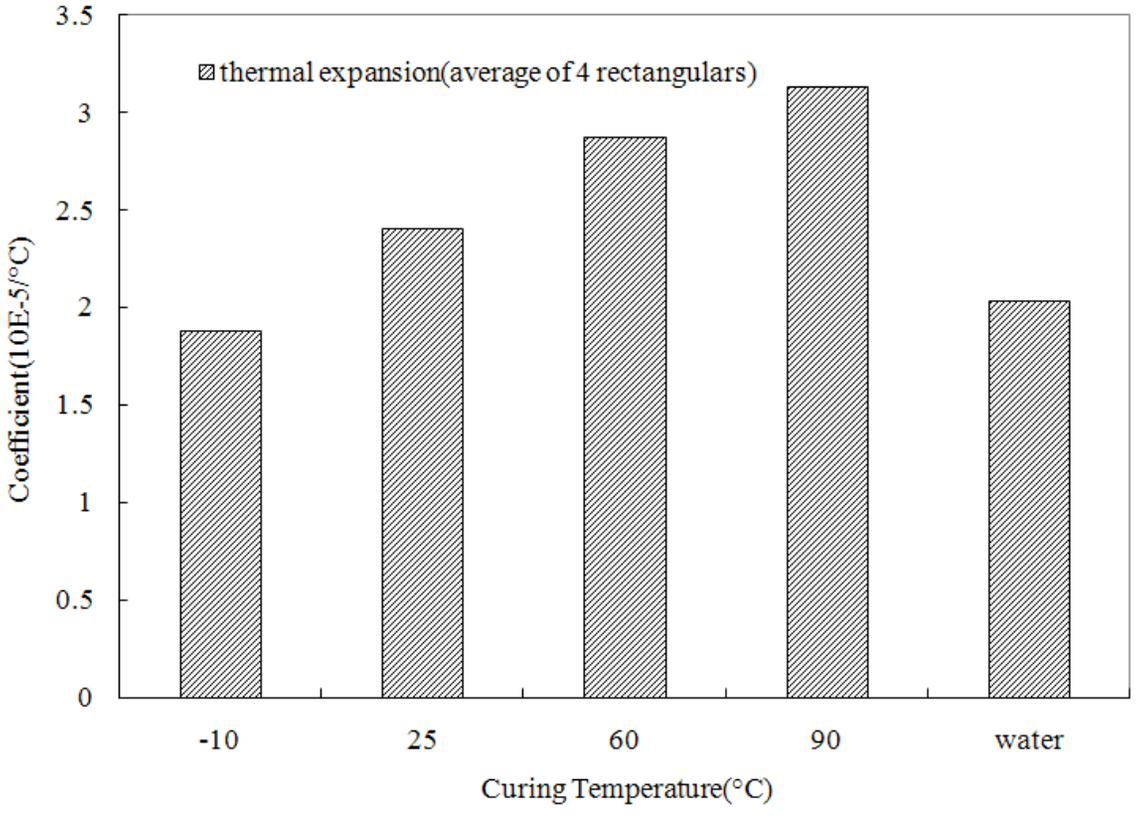

Figure 11. Coefficient of thermal expansion on curing temperature

3.3. Shrinkage behavior

The linear setting shrinkage values of different polymer concrete mixes investigated are presented in Table 6. The shrinkage of recycled unsaturated polyester polymer concrete was generally high, varying between 2400 and 3000 micro strains, as compared to that of Portland cement concrete whose (drying) shrinkage varied usually between 200 and 500 micro strains. However, the measured shrinkage values were in the range of 0.1 ~ 0.3 percent of the reported values were in the range of 0.2 ~ 0.3 percent. The reduced shrinkage values exhibited by the mixes in this study could be due to the use of shrinkage reducer such as montmorillonite.

Montmorillinote Content percent	Resin content percent		
	10	12	15
0	2401	2579	3117
2	2240	2305	2895
4	1938	2014	2405
6	1540	1655	2010
8	1220	1255	1520
10	1225	1250	1530
12	1240	1260	1535

Table 6. Shrinkage values of polymer concrete mixes (micro strains)

The development of shrinkage strains with time for recycled unsaturated polyester polymer concrete mixes containing different filler contents and montmorillonite contents are plotted in Figs. 12 and 13 for mixes made with resin contents 10, 12, 14 and 16 percent, respectively. Shrinkage developed at a rapid rate in the first few hours of casting (4 to 15hr), then slowed down and finally seemed to attain a constant value, with no further or very little increase thereafter, suggesting the near completion of the shrinkage process.

The variation of shrinkage (at 24 hr) with resin and filler contents is plotted in Figs. 14 and 15, respectively. The shrinkage increases linearly with resin content for all proportions of the filler content because the shrinkage of polymer concrete is principally due to its binder content and no shrinkage of the aggregate.

The shrinkage of polymer concrete increases with the filler content also, but the rate of increase seems to decrease at the higher filler content. A possible reason for these increases in shrinkage with filler content could be as below.

As the polymerizing resin shrinks, the aggregate offers a restraint to the shrinkage. Such a restraint is likely to be due to two mechanisms (:) a frictional component at the aggregate surface and the relative low compressibility of the aggregate. The filler, which is very fine and soft, when added, is likely to coat the surfaces of the aggregate particles and cause a decrease in the frictional component of the restraint. In such a case, restraint to shrinkage would decrease as the filler is added. However, when the filler is high (such as 5 percent), the influence of the filler content on polymer concrete is not proportional. This is possible since only a small amount of filler needed to coat the aggregate particles, and the filler content beyond this amount is unlikely to cause a further decrease of the frictional restraint. The low shrinkage of polymer concrete with low resin content and zero filler content has a practical significance in the repair and rehabilitation of deteriorated concrete structures.

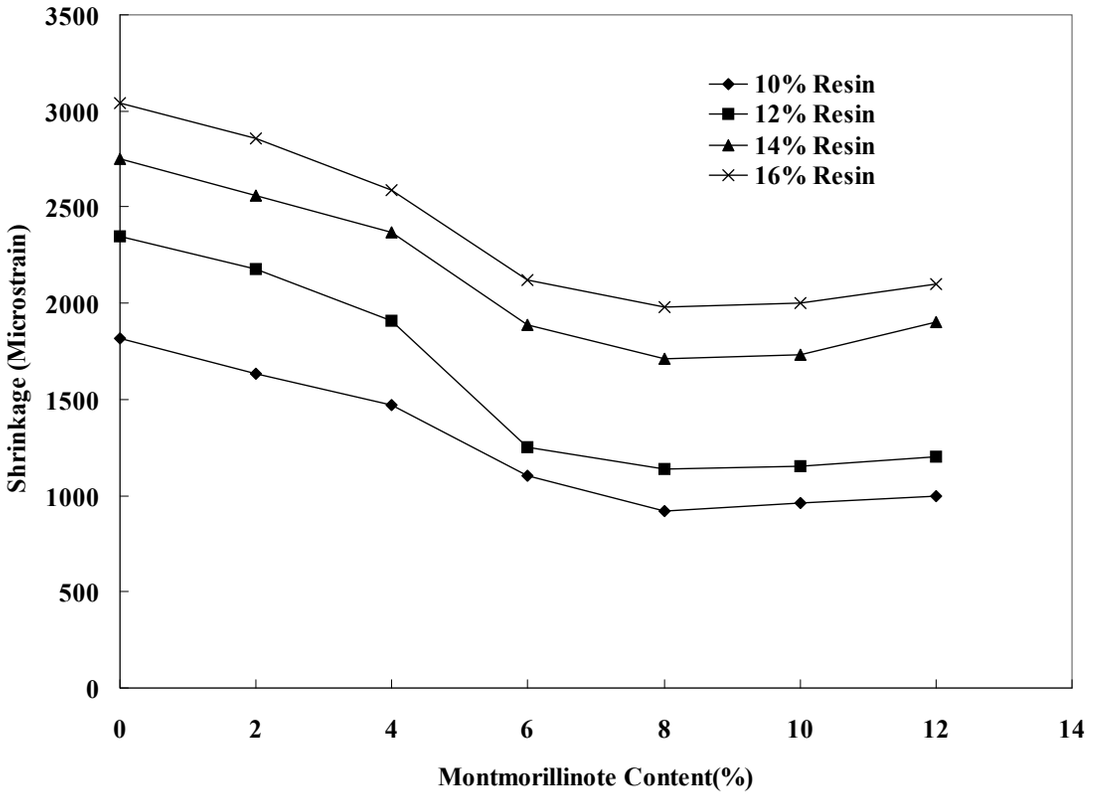

Figure 12. Shrinkage variation of recycled unsaturated polyester polymer concrete with montmorillonite content

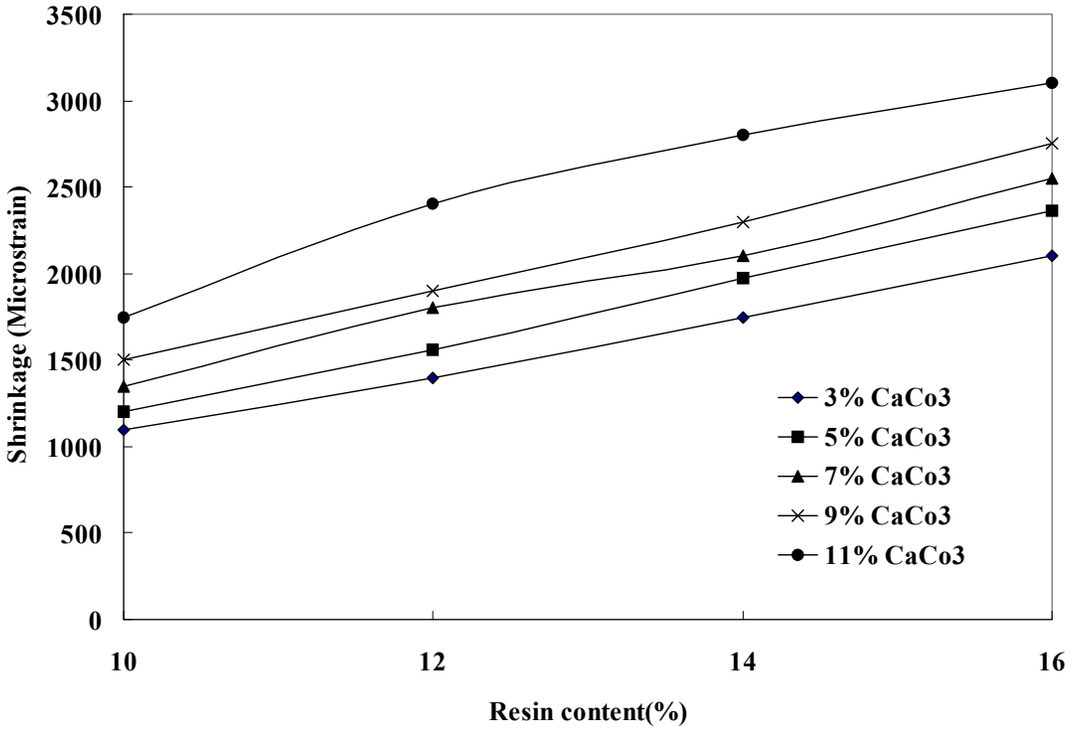

Figure 13. Shrinkage variation of recycled unsaturated polyester polymer concrete with resin content

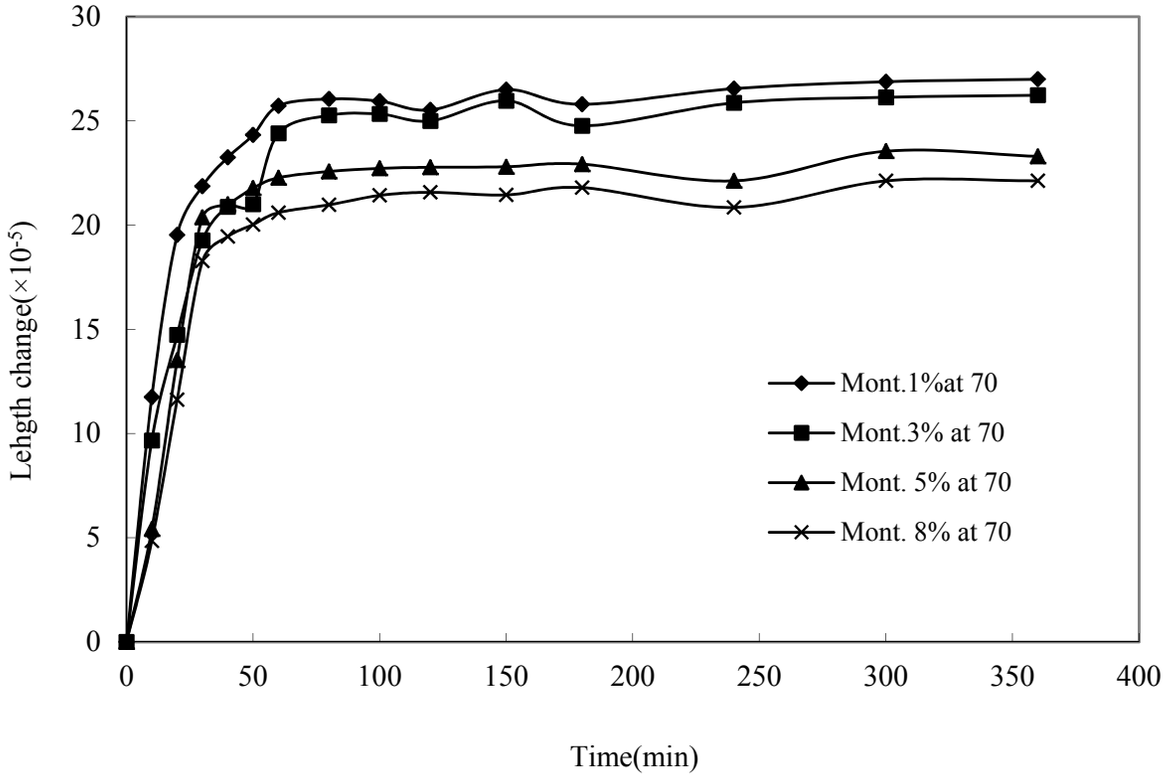

Figure 14. Shrinkage variation of recycled unsaturated polyester polymer concrete with time

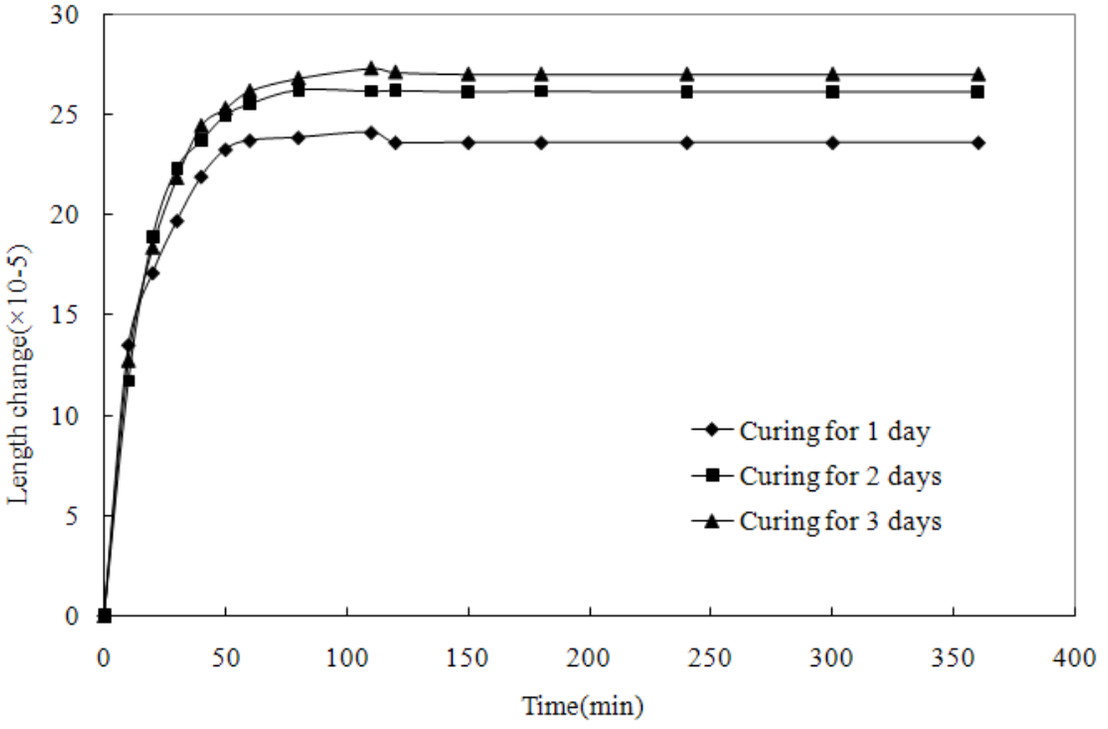

Figure 15. Length change of recycled unsaturated polyester polymer concrete with curing days

3.4. Prediction of long-term creep behavior

The short-term creep tests provided the 24 hour creep compliance values at the temperatures (20°C, 30°C and 40°C) to construct a Prony series equation that predicts the long-term creep compliance at the 20°C temperature.

The proposed method of short-term creep tests was used to predict the long-term creep compliance of recycled PET polymer concrete, incorporating types of filler, stress ratio and filler content. Each creep compliance curve is represented by the following Prony series equation:

$$D(t) = D_g + D_1(1 - e^{-t/24}) \tag{11}$$

where D_g, the glassy creep compliance, is the creep compliance at t=0 hours. The coefficient D_1, which is a function of the glassy compliance D_g, and the 24-hour creep compliance $D(24)$ are determined by Eq. (11). The values of the Prony series coefficients D_g, D_1 for compressive short-term creep tests performed on polymer concrete are shown in Tables 7 and 8. The 24-hour creep factor, $f(24)$, that is, the ratio of the specific creep $D(24) - D_g$ to the glassy compliance D_g, is also shown in Tables 7 and 8.

The coefficients of the Prony series that represents the short-term creep curves, shown in Tables 7 and 8, were used to calculate the coefficients of the following Prony series equation predicting the long-term compliance at the 20°C creep curve:

PC System	Temp. (°C)	$D(0) = D_g$ (μ/Mpa)	$D(24)$ (μ/Mpa)	D_1 (μ/Mpa)	$f(24)$
F-C-L20	20	204.60	223.91	30.55	0.094
	30	223.51	257.30	53.45	0.151
	40	260.00	332.60	114.85	0.279
F-Fa-L20	20	218.91	241.10	35.10	0.101
	30	240.98	275.85	55.16	0.145
	40	278.24	356.60	123.96	0.279
F-N-L20	20	328.79	369.67	64.67	0.124
	30	368.19	439.10	112.18	0.193
	40	437.36	592.70	245.74	0.355
F-C-L30	20	214.30	237.32	36.42	0.107
	30	237.89	276.86	61.65	0.164
	40	275.34	358.80	132.30	0.304
F-C-L40	20	247.34	277.32	47.43	0.121
	30	278.42	327.91	78.32	0.184
	40	322.30	431.91	173.40	0.340
F-C20-L20	20	200.11	219.30	30.37	0.096
	30	217.92	241.50	37.30	0.108
	40	239.67	280.20	64.12	0.169
F-C30-L20	20	195.58	211.50	25.19	0.081
	30	219.14	245.80	42.18	0.122
	40	243.14	284.80	65.91	0.171

Table 7. Results of short-term creep test

PC System	r	D_g^{20}	D_1^{20}	D_1^{30}	D_1^{40}
F-C-L20	0.862	204.60	30.55	46.07	99.00
F-Fa-L20	0.906	218.91	35.10	49.97	112.30
F-N-L20	0.811	328.79	64.67	90.98	199.30
F-C-L30	0.865	214.30	36.42	53.33	114.44
F-C-L40	0.842	247.34	47.43	65.95	146.00
F-C20-L20	1.272	200.11	30.37	47.45	81.56
F-C30-L20	1.110	195.58	25.46	46.82	73.16

Table 8. The coefficients of Prony series equation

$$D(t) = D_g^{20} + D_1^{20}(1 - e^{-t/24}) + rD_1^{30}(1 - e^{-t/1000}) + rD_1^{40}(1 - e^{-t/6000}) \quad (12)$$

where D_g^{20} and D_1^{20} are the coefficients of the Prony series equation that represents short-term creep curve at the 20°C temperature. The last two terms of Eq. (12), which constitute the prediction terms, are determined from the results of the short-term creep tests performed at elevated temperatures (30°C and 40°C).

Coefficients D_1^{30}, and D_1^{40} of Eq. (12) are the Prony series coefficients that correspond to short-term creep curves at the 30°C and 40°C temperature. The factor r is used to adjust the coefficient so that the error in the predicted creep compliance may be minimized. Different values of r were substituted in Eq. (12) in order to define the range of r for which the error is minimized. A single value of r does not minimize the error of the predicted creep compliance in all polymer concrete. We determined the value of r to minimize the error of the results of the short-term creep tests performed at the 30°C, 40°C temperature. It was observed that the values of r for which the error was minimized could be related to the ratio of the Prony series coefficients and the average creep factor of all temperatures f_{ave} by

$$r = \frac{D_1^{20}}{D_1^{30}} + \frac{D_1^{30}}{D_1^{40}} - f_{ave} \quad (13)$$

where D_1^{20}, D_1^{30}, D_1^{40}, and f_{ave} are listed in Table 8. The ratios of the coefficient in Eq. (13) represent the compliance curves. The ratio D_1^{20} to D_1^{30}, for example, is the slope ratio of the 20°C and 30°C creep curve at the 24 hour. This can be proved by using the first derivatives of Eq.3 and Eq.4, which represent the short-term creep compliance curves at the 20°C, 30°C temperature. The values of r shown in Table 8 were determined by Eq. (13).

The values of r, determined by Eq. (13), and the other coefficients of Eq. (12) display the coefficients of a different Prony series equation. The Prony series equation that predicts the compressive long-term creep compliance of the F-C-L20, for example, is constructed by using the values listed in the first row, as follows:

$$D(t) = 204.6 + 30.55(1 - e^{-t/24}) + 46.07(1 - e^{-t/1000}) + 99(1 - e^{-t/6000}) \quad (14)$$

3.5. Evaluation of the short-term creep test

The creep compliance curves that were predicted using the Prony equations, and experimental creep compliance curves, are shown in Figs. 16, 17, and 18. It shows the creep compliance curves of polymer concrete systems on the 20, 30, and 40% stress ratio namely F-C-L20, F-C-L30 and F-C-L40. The curves of the F-C-L30 and F-C-L40 are one year long.

The differences between the predicted and the experimental creep compliance curves that are shown in Figs. 16,17 and 18 were caused by: (1) the differences between the glassy modulus of the short-term creep test and the glassy modulus of the long-term creep test,

and (2) the inaccuracy of the prediction method. The error that was caused by the inaccuracy of the prediction method was isolated by subtracting the glassy creep compliance from both the predicted and the experimental creep compliance values.

A more accurate evaluation is made by a quantitative comparison of the results. The predicted specific creep and creep compliance values are compared in Table 9 with the corresponding experimental values obtained from a long-term creep test. The difference between the predicted and the experimental values is expressed as a percentage of the experimental values.

The errors of the predicted creep compliance values, shown in Table 9, are less than 5 percent for all polymer concrete systems.

The difference between the two curves is due to differences between the glassy compliance of short-term creep test and the long-term creep test at the 20°C temperature. The difference in the glassy compliance was probably caused by a small difference in the elastic modulus of the polymer concrete that was not cast at the same time.

The minor difference between the predicted and the experimental creep strains indicates that the short-term creep test can be successfully used to predict the long-term creep deformation of the polymer concrete systems examined.

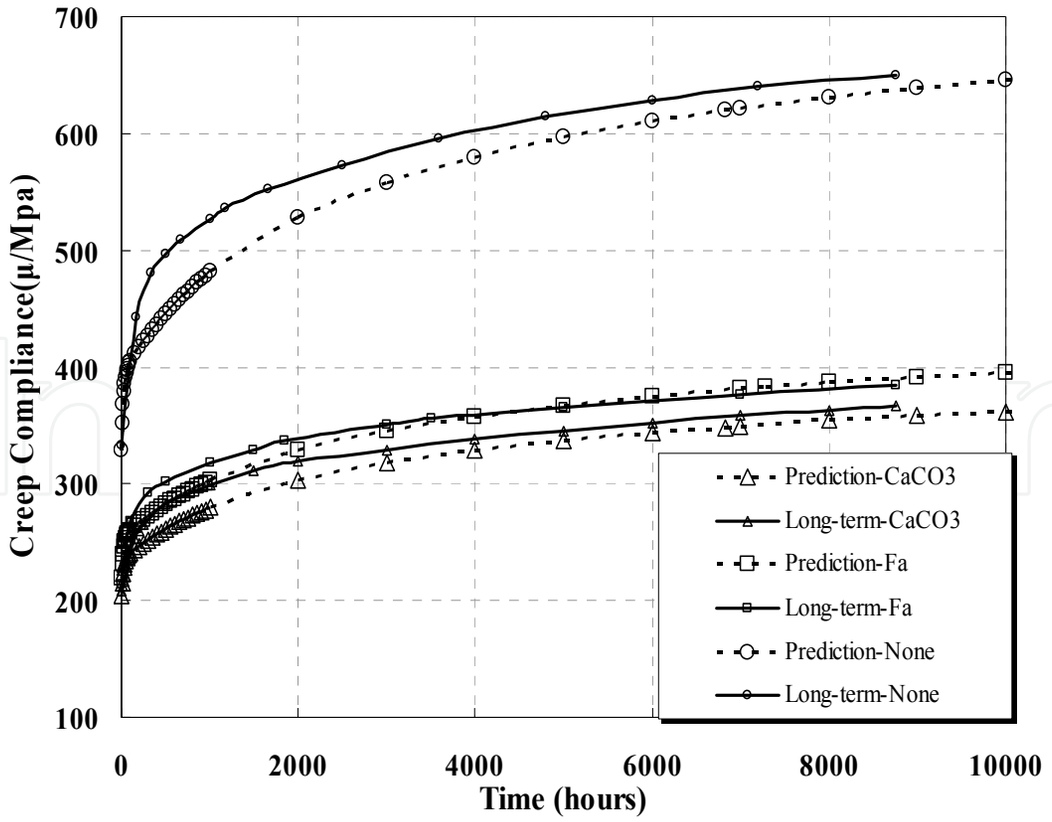

Figure 16. Creep compliance curves depending on filler types

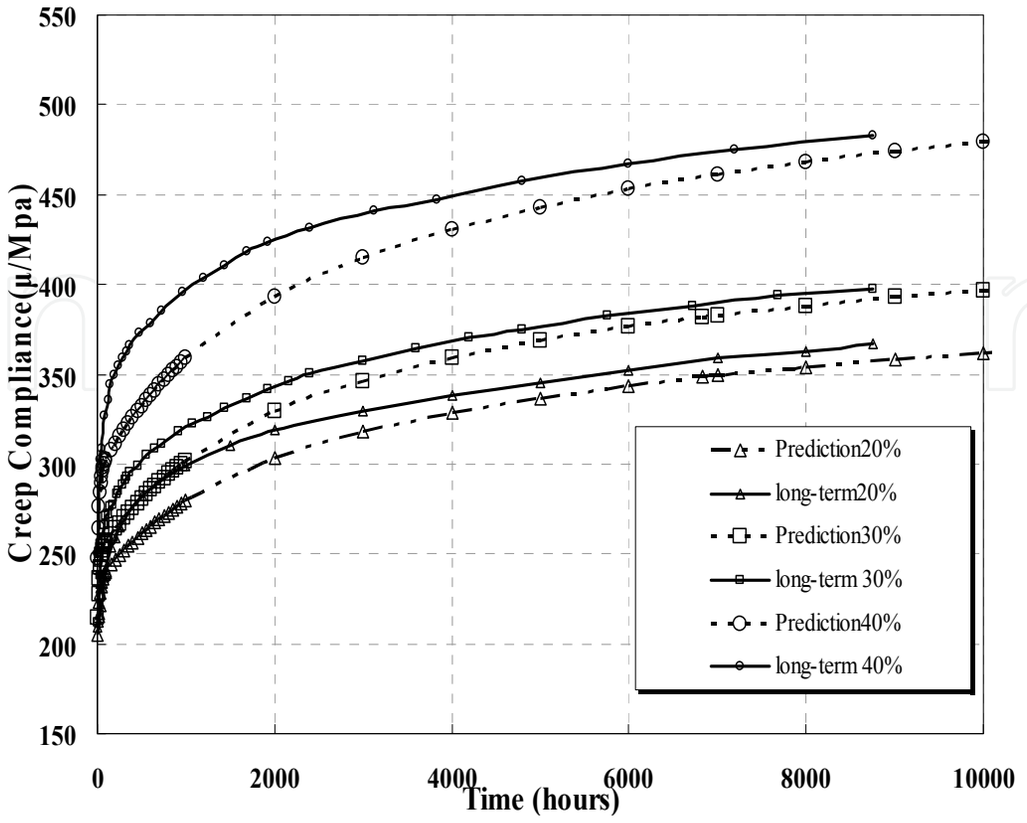

Figure 17. Creep compliance curves with stress ratios

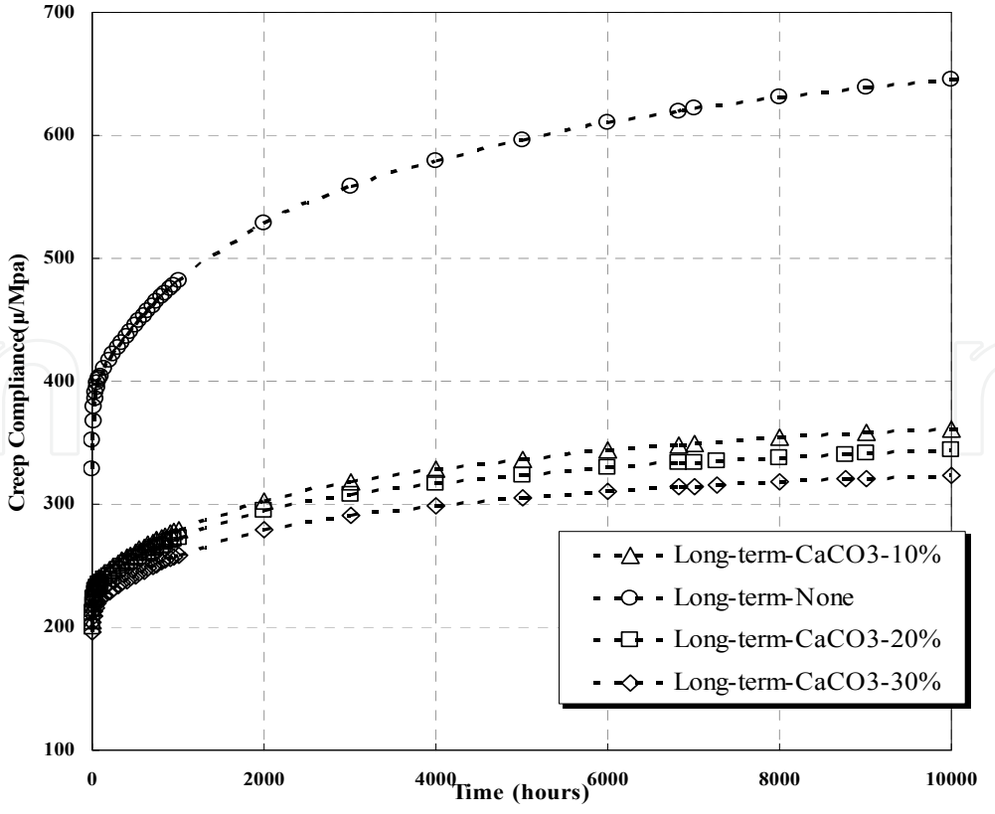

Figure 18. Creep compliance curves depending on filler contents

PC System	Creep Compliance			Specific Creep		
	Pred. (μ/Mpa)	Exp. (μ/Mpa)	Err. (%)	Pred (μ/Mpa)	Exp. (μ/Mpa)	Err. (%)
F-C-L20	358.1	366.9	2.5	152.6	157.9	3.5
F-Fa-L20	390.2	383.9	-1.6	171.3	169.5	-1.1
F-N-L20	637.4	650.0	2.1	308.7	316.4	2.5
F-C-L30	391.9	397.5	1.4	177.6	186.0	4.7
F-C-L40	472.8	482.7	2.1	225.5	232.7	3.2

Table 9. Comparison of the prediction and experimental creep

3.5.1. Effect of filler type

The filler plays an important role in restricting the deformation of polymer concrete. The filler decreases the quantity of resin per unit volume at mixing, and increases adhesion by increasing the viscosity [19].

In this study, resin and applied stress were fixed while different types of filler were used. Creep strain and specific creep prediction curves on the type of filler are shown in Figs. 19 and 20.

The creep strains were 394.87μ with the $CaCO_3$ and 433.9μ with the fly-ash, by prediction equation. The creep strain and specific creep were found to be smaller when $CaCO_3$ was used than when fly-ash was. The long-term creep strain of $CaCO_3$ was 408.52μ and that of fly-ash was 429.4μ.

The heavy calcium carbonate has a greater specific surface area than fly-ash. So, it has more bonding area with resin binder than the fly-ash does. Therefore, the adhesion between the resin binder and the aggregates is stronger, reducing creep strain. Fineness of fly-ash is smaller than that of $CaCO_3$, approximately 2,800 cm^2/g and 3,765cm^2/g respectively.

Very small fineness interrupts the cross-linking between the resin binder and the aggregates during polymerization. The adhesions decrease in the interface between the aggregates. Reduction of adhesion causes weak restriction of the resin, increasing creep deformation.

The creep strain of F-N-L20, which did not use the filler, is dramatically increased. This illustrates the importance of the filler in restricting the resin's deformation. The predicted creep strain and the specific creep (without filler) were 557.94μ and 308.65μ. The creep strain of the concrete without a filler thus approximately 30 percent to 40 percent higher than that with a filler. The specific creep was about two times higher than with a filler.

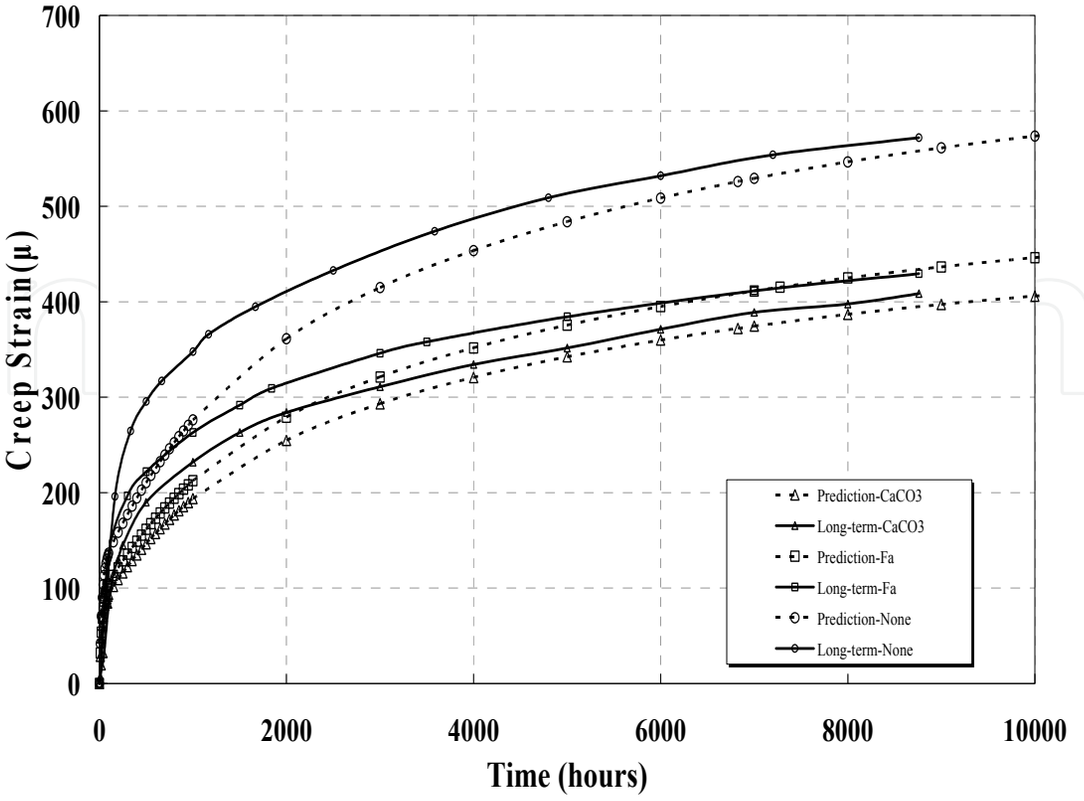

Figure 19. Creep strain curves depending on filler types

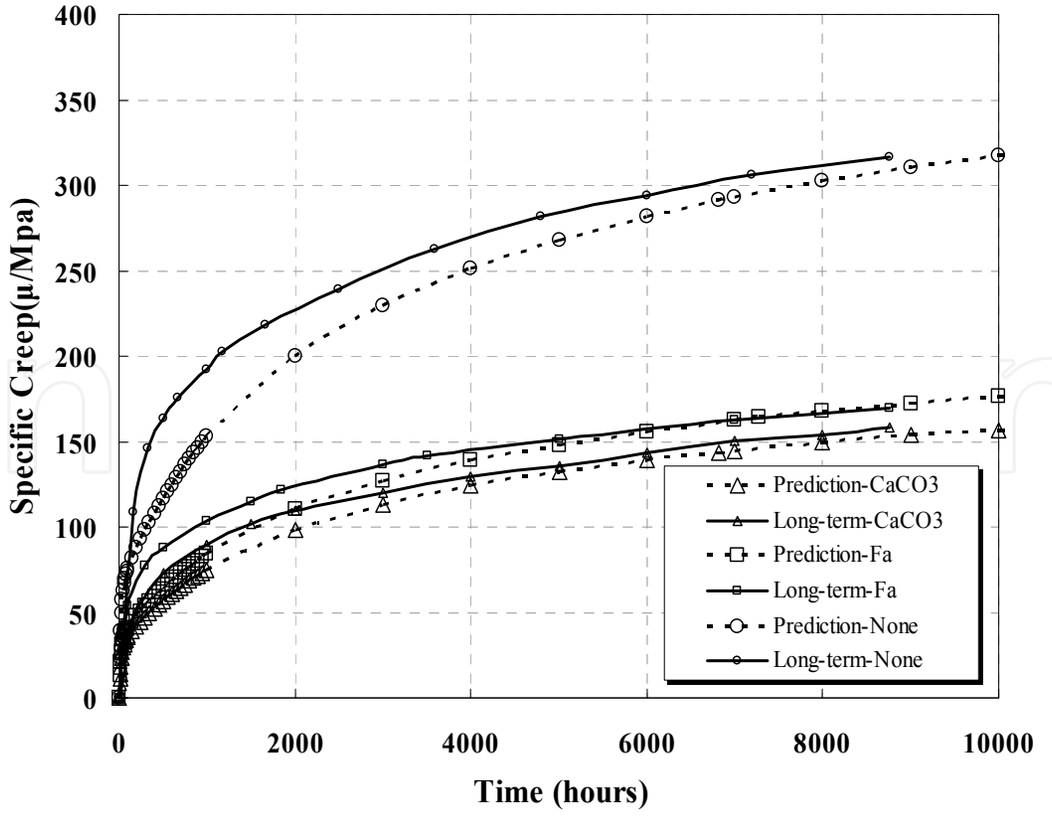

Figure 20. Specific creep curves depending on filler types

3.5.2. Effect of the stress ratio

The resin and filler contents were constant and the polymer concrete systems were subjected to progressively increasing stress ratios, ranging from 0.2 to 0.4 of the ultimate compressive strength. Creep strain and specific creep prediction curves on the stress ratio are shown in Figs. 21 and 22. In comparison with the predictions given by the Prony series equation, the creep strain and the specific creep curves given by the prediction curves are slightly lower than those of the long-term creep curves.

In the prediction creep strain, more than 20 percent of the final creep took place within the first two days and nearly 50 percent during the first 20 days, as shown in Fig. 21. In the long-term creep strain, however, 20 percent of the final creep was measured within first 1.5 days and 50 percent during the first 20 days. On the other hand, in the case of conventional concrete, 25 percent of the final creep takes place within the first month of loading and 50 percent within the first 3 months.

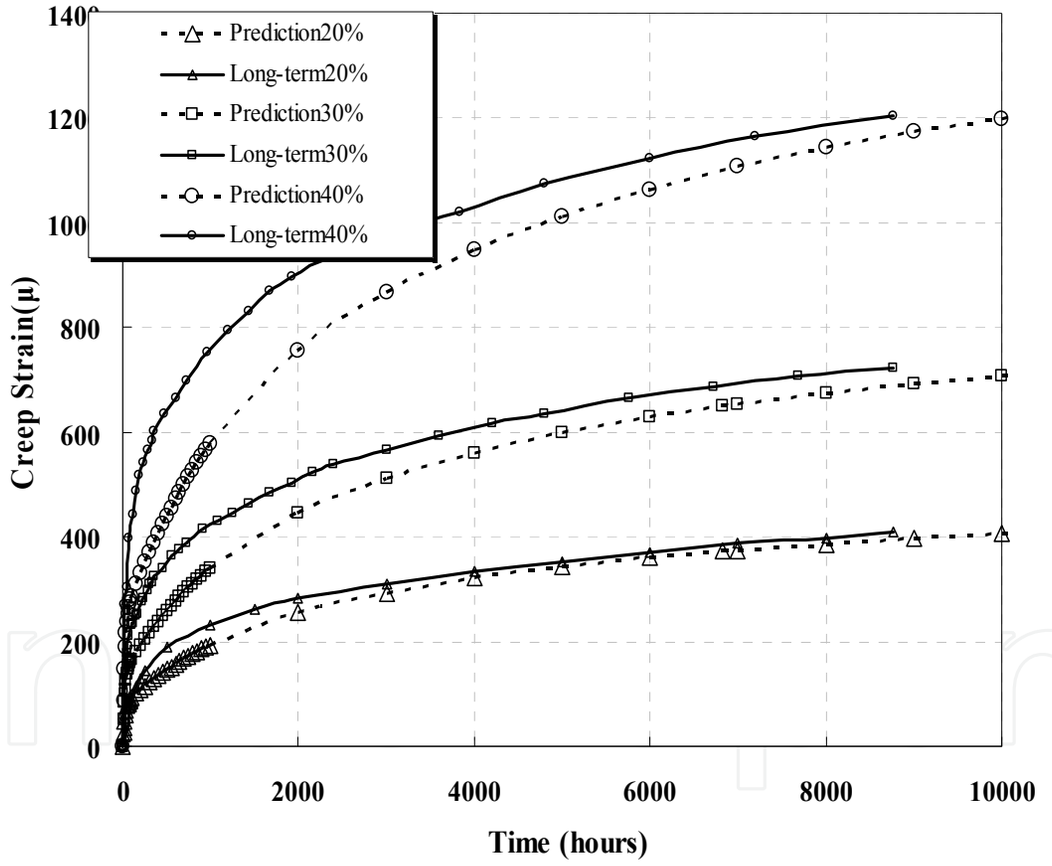

Figure 21. Creep strain curves with stress ratios

The prediction creep curves are smaller than long-term creep curves at an early stage, although the prediction creep strains are approximately equal to long-term creep at one year. After the rapid increase in strains at the early stages of loading, the deformation decreased and the creep strain curves tend to level off after approximately the first two to three months of applied load.

As expected, a higher stress ratio resulted in a larger creep strain. However, in comparison with the stress ratio results, the creep strain is not proportional to the rate of stress increase. During the first year, the prediction creep strain and long-term creep strain were 394.87μ and 408.53μ at 0.2, 689.35μ and 722μ, at 0.3, and 1166.65μ and 1204μ at 0.4 stress ratio. As the applied stress increased about 50 percent, the creep strain increased 75 percent. It increased 190 percent as the applied stress rose up to 100 percent. The specific creep, the creep strain per unit applied stress, is shown in Fig. 22.

The prediction and the long-term specific creep, at one year, are 152.62μ/Mpa and 157.9μ/Mpa at 0.2, 177.6μ/Mpa and 186μ/Mpa at 0.3, and 225.45μ/Mpa and 232.6μ/Mpa at 0.4 stress ratio. The trend of specific creep is approximately equal to the creep strain, regardless of the stress ratio. Creep behavior of polymer concrete using recycled polyester resin is viscoelastic behavior.

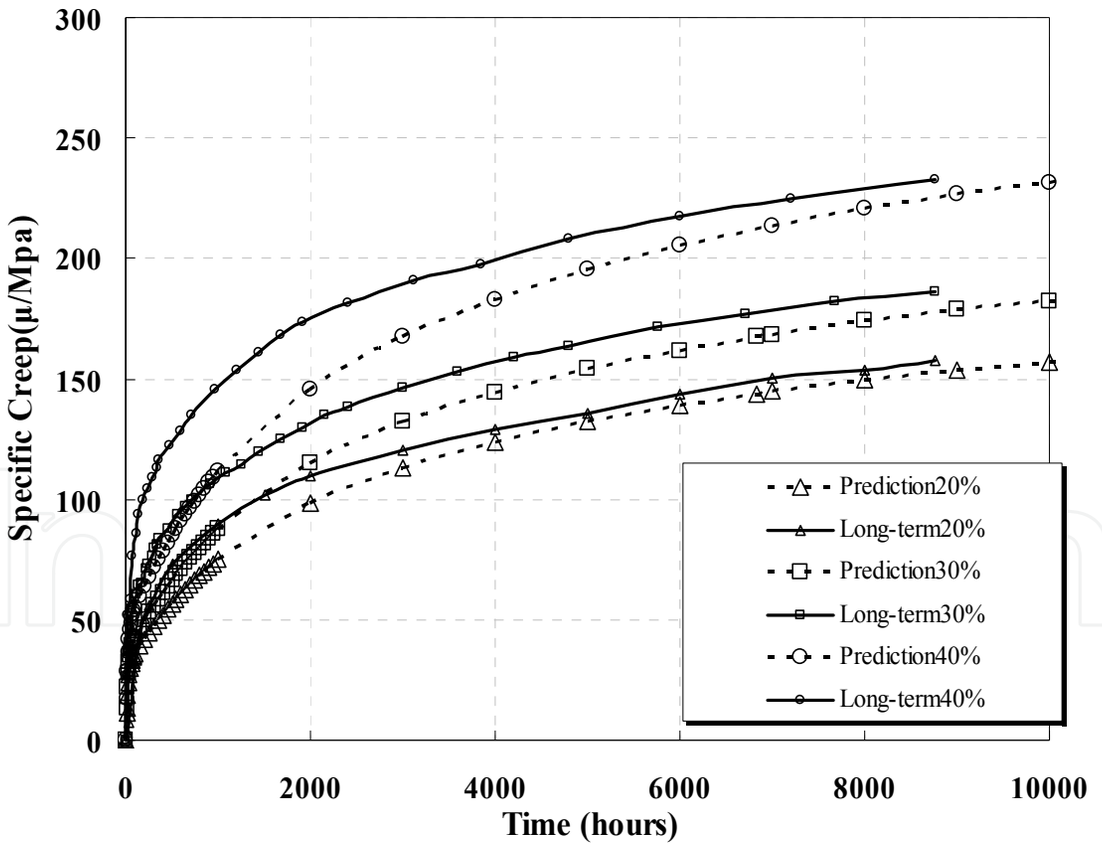

Figure 22. Specific creep curves with stress ratios

3.5.3. Effect of filler contents

In this study, the resin content and stress ratio were fixed and the filler contents ($CaCO_3$) varied from 0 to 30%. The creep strain and the specific creep prediction curves on the contents of filler are shown in Figs. 23 and 24. The predicted creep strains and specific creeps are 557.94μ and 308.65μ/Mpa without filler, 394.87μ and 152.62μ/Mpa with 10% filler, 343.99μ and 140.43μ/Mpa with 20%, and 341.27μ and 125.17μ/Mpa with 30% by prediction equations. In comparison with the results, it is clear that as the filler content increased, the creep strain and the specific creep decreased. As the filler content increased from 10 to 20 percent, the specific creep decreased about 8 percent. As it increased from 20 to 30 percent, the specific creep rose about 11 percent. As it increased from 0 to 10 percent, the specific creep decreased about 50 percent. This indicates that the use of filler had more of an effect than filler content.

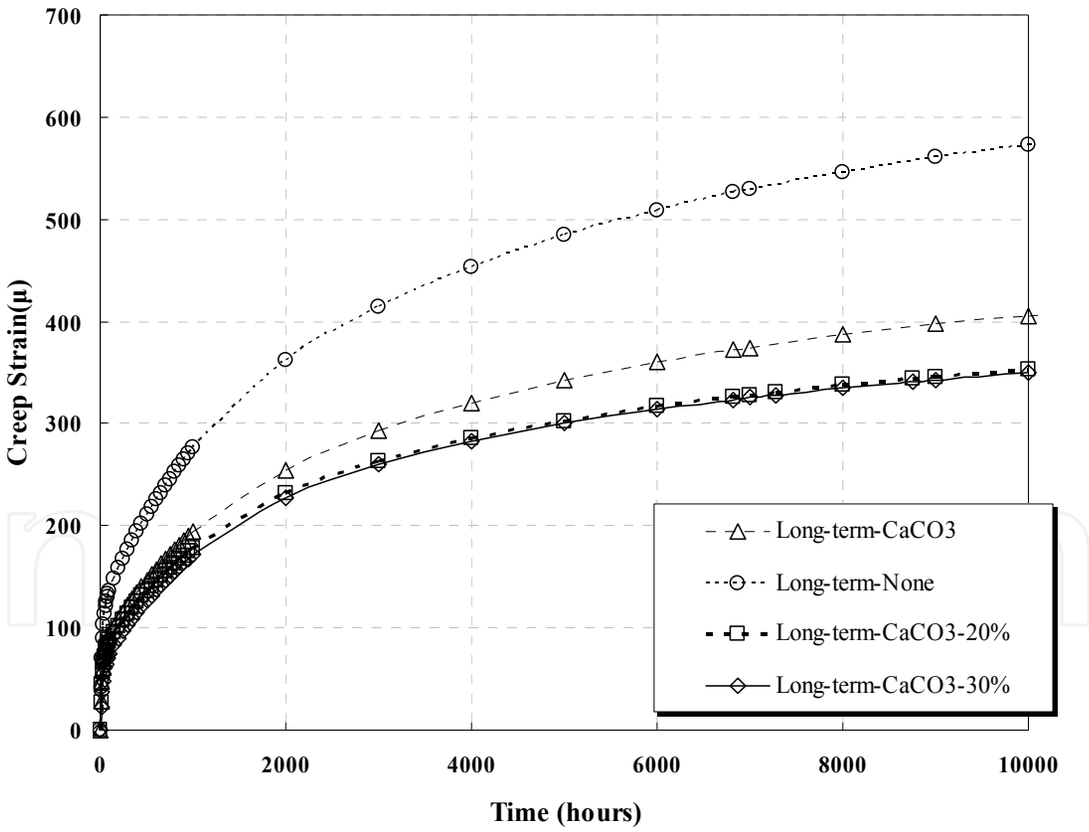

Figure 23. Creep strain curves depending on filler contents

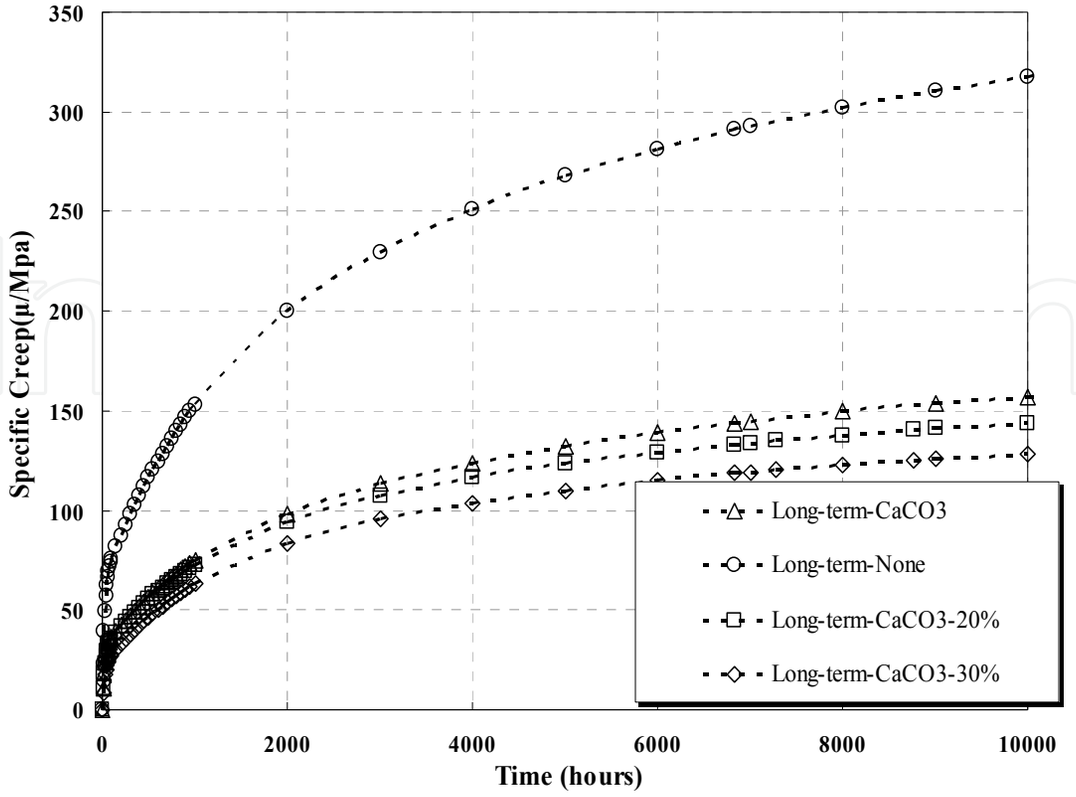

Figure 24. Specific creep curves depending on filler contents

4. Conclusion

Based on the results obtained in this investigation on time dependent behavior of polymer concrete, the following conclusions can be drawn:

1. Strength test results revealed that the material could achieve more than 85% of its final strength in one day. This result is an important advantage in many construction and structural applications. The material experiences a loss in strength at high temperatures; this result may be important if the polymer concrete is used in precast box culvert, for example. However, despite this loss in strength at high temperatures, the material remains strong compared to portland cement concrete.
2. Montmorillonite considerably affect various properties of polymer concrete. Also, the more the montmorillonite content increases, the more both the setting shrinkage and sensitivity to heat decrease. This result shows that montmorillonite without a special coupling agent could be used as one of the additives to enhance various properties of polyester resin.
3. The coefficient of thermal expansion of fly ash was relatively lower than that of calcium carbonate because similar chemical composition led to active reaction with montmorillonite.
4. With the addition of montmorillonite 5%, the compressive strength was found to increase by 12%. Improvements in the properties of recycled unsaturated polyester polymer concrete were true for the optimum values of 5% of montmorillonite content. If

the percentage of the montmorillonite exceeds 5%, recycled unsaturated polyester polymer concrete properties either remain constant or change in a negative way.

5. The long-term creep prediction models are formulated to facilitate an understanding of the behavior of polymer concrete structures through short-term creep tests. The error between the long-term creep prediction and experimental long-time creep compliance is so negligible as, less than about 4%.
6. The creep strains grow rather fast at early ages in comparison with ordinary concrete, because creep in polymer concrete results from molecular movement in the viscoelastic resin binder. The recycled-polymer concrete shows more than 20% of its long-term creep within the first two days, and about 50% during the first 20 days.
7. The creep strain of polymer concrete without a filler is much higher than that of polymer concrete with a filler, because the filler plays an important role in restricting the deformation of polymer concrete. Also, as far as the type of filler is concerned, the effect of $CaCO_3$ as a filler on polymer concrete is better than that of fly-ash in terms of the creep strain and specific creep. This is attributed to the larger surface area of $CaCO_3$ particles and the higher adhesion between the resin binder and the aggregates.

Author details

Ghi Ho Tae
Department of Structural Engineering, Seoul National University of Science & Technology, Korea

Eun Soo Choi
Department of Civil Engineering, Hongik University, Korea

5. References

[1] ACI Committee 548, "Guide for the use of Polymers in Concrete", *ACI Materials Journal*, V. 82, No. 5, September 1997, pp.11~13

[2] Vaidya, U.R.,and Nadkarni, V.M., "Unsaturated Polyester Resins from Poly(ethylene terephthalate) Waste", Industrial & Engineering Chemistry Research, Vol.26, 1987, pp.194-198

[3] Rebeiz, Karim Sami, "Structural use of Polymer Composites using Unsaturated Polymer Resins based on Recycled Poly(ethylene terephthalate)", Ph.D. at Austine in Texas, 1992, pp.59~62

[4] Edith A. Turi, "Thermal Characterization of Polymeric Materials", 2nd Edition Vol. 1, Academic Press, 1997, pp.227 pp.1145

[5] K.S.Rebeiz, "Precast Use of Polymer Concrete using Unsaturated Polyester Resin based on Recycled PET waste", *Construction and Building Materials* Vol.10 No.3, pp.216 ~ 218

[6] Kim ju hyeon, "A Study on the Strecture-Property Relationships of Unsaturated Polyester Resins Based on Recycled PET", Ph. M. in Chonbuk Uni, February 1995, pp.17-20, 49 ~ 50

[7] Peschke, H.J., "Stress and Strain Analysis Between Cementitious Concrete and Polymer Concrete", 3th ICPIC, pp.477 ~ 489
[8] Karim S.Rebeiz, "David W.Fowler and Donald R.Paul, Mechanical Properties of Polymer Concrete Systems Made with Recycled Plastic", *ACI Material Journal* V.91, No.1, Jan-Feb 1994, pp.40 ~ 45
[9] David Stanley, "Investigation of Dow Polyesteramide Resins for Use in Polymer Concrete", The University of Texas at Austin, 1984, pp.65 ~ 68
[10] C.E.Bream and P.R.Hornsby, "Structure Development in Thermoset Recycled-Filled Polypropylene Composites", Journal of Polymer Composites, June 2000, Vol.21, No.3, pp.418 ~ 423
[11] Dae-Keun Park and Jin-Hae Chang, "Nanocomposites Based on Montmorillonite and Thermotropic Liquid Crystalline Polyester", The Journal of Polymer, May 2000, Vol. 24, No.3, pp.339 ~ 406
[12] Scuk-Hyun Lee, "A Study on the Swelling Behavior of a Cured Unsaturated Polyester", *The Journal of Polymer*, December 1987, Vol. 11, No. 6, pp.557 ~ 562
[13] Alkonis, J. J., Maxknight, W. J., Shen, M., "Introduction to Polymer Viscoelasticity," Wiley-Interscience, John Wiley & Sons, INC., New York, 1972.
[14] E. Riande, R. Diaze-Calleja, Margarita G. Prolongo, Rosa M. Masegosa, Catalina Salom "Polymer Viscoelastisity Stress and Strain in Practice," Marcel Dekker, INC. 2000.
[15] Hsu, M., Fowler, D.W, "Creep and Fatigue of Polymer Concrete," Polymer Uses-Materials and Properties, ACI, SP 89-17, pp. 323~343, 1985.
[16] J.-P. Boehler, T. Dietl, A. Millien, "Creep Law for Polymer Concrete in the Hardening State"
[17] John D. Ferry, "Viscoelastic Properties of Polymers," third edition, John Wiley & Sons, INC, 1980.
[18] K. Aniskevich, J. Hristova, "Aging and Filler Effects on the Creep Model Parameters of Thermoset Composites," Composite Science and Technology, Vol.62, pp. 1097~1103, 2002.
[19] K. Aniskevich, J. Hristova, "Creep of Polyester Resin Filled with Minerals," Journal of Applied Polymer Science, Vol. 77, pp. 45~53, 2000.
[20] K. S. Rebeiz, "Time-Temperature Properties of Polymer Concrete Using Recycled PET," Cement&Concrete Composites Vol.17 pp.119~124, 1995.
[21] K. K. Charalambous, "Accelerated compression and flexural creep testing of polymer concrete", Ph.D. Dissertation, University of Texas at Austin, 1991.